nature

https://doi.org/10.1038/s41586-025-09932-w

Accelerated Article Preview

CD8$^+$ T cell stemness precedes post-intervention control of HIV viremia

Received: 20 April 2025

Accepted: 18 November 2025

Accelerated Article Preview
Published online: 01 December 2025

Cite this article as: Kiani, Z. et al. CD8$^+$ T cell stemness precedes post-intervention control of HIV viremia. *Nature* https://doi.org/10.1038/s41586-025-09932-w (2025)

Zahra Kiani, Jonathan M. Urbach, Hannah Wisner, Mpho J. Olatotse, Daniel Y. Chang, Joshua A. Acklin, Alicja Piechocka-Trocha, Nathalie Bonheur, Ashok Khatri, Mathias Lichterfeld, Jesper D. Gunst, Ole S. Søgaard, Marina Caskey, Michel C. Nussenzweig, Bruce D. Walker & David R. Collins

CD8$^+$ T cell stemness precedes post-intervention control of HIV viremia

Zahra Kiani[1,10], Jonathan M. Urbach[1,10], Hannah Wisner[1,10], Mpho J. Olatotse[1], Daniel Y. Chang[1,2], Joshua A. Acklin[1], Alicja Piechocka-Trocha[1,3], Nathalie Bonheur[1], Ashok Khatri[4], Mathias Lichterfeld[1,5], Jesper D. Gunst[6,7], Ole S. Søgaard[6,7], Marina Caskey[8], Michel C. Nussenzweig[3,8], Bruce D. Walker[1,3,9], David R. Collins[1,3]*

[1] Ragon Institute of Mass General Brigham, MIT and Harvard, Cambridge, MA, USA

[2] Department of Pathology, Mass General Brigham, Boston, MA, USA

[3] Howard Hughes Medical Institute, Chevy Chase, MD, USA

[4] Mass General Brigham Peptide Research Core, Massachusetts General Hospital, Charlestown, MA, USA

[5] Division of Infectious Diseases, Brigham and Women's Hospital, Boston, MA, USA

[6] Department of Infectious Diseases, Aarhus University Hospital, Aarhus, DK

[7] Department of Clinical Medicine, Aarhus University, Aarhus, DK

[8] Laboratory of Molecular Immunology, The Rockefeller University, New York, NY, USA

[9] Institute for Medical Engineering and Science and Department of Biology, Massachusetts Institute of Technology, Cambridge, MA, USA

[10] These authors contributed equally

* Corresponding author: drcollins@mgh.harvard.edu

Interventions to induce lasting HIV remission are needed to obviate the requirement for lifelong antiretroviral therapy (ART). Durable post-intervention control (PIC) of viremia has been achieved in a subset of individuals following broadly neutralizing anti-HIV-1 antibody (bNAb) administration and analytical treatment interruption (ATI)[1-4]. Prior studies support a role for CD8$^+$ T cells[5-9] but the precise features of CD8$^+$ T cells involved in PIC remain unclear. Here we mapped and functionally profiled CD8$^+$ T cell responses to autologous HIV epitopes using longitudinal samples from four ATI trials in bNAb recipients. PIC was associated with superior pre-intervention HIV-specific CD8$^+$ T cell proliferative capacity, stem cell-like memory phenotype, and recall cytotoxicity against autologous HIV peptide-pulsed CD4$^+$ T cells. CD8$^+$ T cell stemness was further increased following bNAb administration without emergence of new clonotypes targeting defined HLA-optimal epitopes. Multimodal single-cell analyses revealed molecular features associated with PIC and HIV-specific CD8$^+$ T cell stemness, including signatures of metabolic fitness and reduced T cell exhaustion. These results identify immune features that precede subsequent PIC to inform the development of combination immunotherapies that will elicit durable HIV remission.

MAIN TEXT

Approximately 40 million people worldwide are living with HIV, requiring lifelong antiretroviral therapy to prevent recrudescent viral replication, transmission, and disease progression[10]. To inform the development of a functional cure by which durable ART-free remission can be achieved, mechanisms underlying spontaneous control of HIV to undetectable levels without ART have been extensively studied[11,12]. The proliferative capacity of HIV-specific memory CD8$^+$ T cells has been repeatedly linked to spontaneous control[13-15], is associated with increased stemness[16], and facilitates lytic granule loading for cytotoxic elimination of HIV-infected cells[17]. Moreover, loss of these functions precedes aborted spontaneous control of HIV[18].

A small fraction of people with HIV (PWH) can maintain low or undetectable plasma viral loads for a variable period following discontinuation of ART[19,20]. Specifically, 4% of participants in noninterventional ATI trials achieved control of viremia for 84 days or more[21]. Such post-treatment control (PTC) has been associated with particular virologic and immunologic characteristics, such as smaller persistent HIV reservoirs, autologous virus neutralization, and reduced T cell activation[22-24], while precise determinants remain under investigation. Efforts to achieve durable post-ART control in a larger proportion of PWH have combined ATI with interventions such as passive bNAb infusion[1-4,25]. Although post-intervention control (PIC) of viremia has been achieved following bNAb administration at higher rates than PTC in noninterventional trials, a majority of bNAb recipients still failed to control viremia, highlighting the need for a deeper understanding of immune responses that mediate PIC[26]. Control of viremia following bNAb administration in non-human primates was lost upon depletion of $CD8^+$ T cells[5-7], demonstrating their importance in PIC. While modest augmentation of virus-specific $CD8^+$ T cells has been observed *in vivo* following bNAb administration[5-9], the precise $CD8^+$ T cell features and functions associated with PIC and the extent to which their augmentation facilitates PIC remain unclear.

Here we identify immune correlates preceding subsequent PIC by studying $CD8^+$ T cell responses targeting autologous HIV epitopes in longitudinal specimens obtained from participants of four similar interventional trials. PIC was not associated with broadening of HIV-specific responses against autologous HLA-optimal epitopes following bNAb administration but was significantly associated with superior pre-intervention proliferative and cytolytic potential of HIV-specific stem cell-like memory $CD8^+$ T cells. These responses were further enhanced following bNAb administration and were associated with changes in metabolic gene expression. These immune correlates of PIC may inform strategies to elicit ART-free control of viremia in a larger proportion of PWH.

PIC is not associated with broadening of CD8⁺ T cell responses

We obtained longitudinal peripheral blood mononuclear cells (PBMCs) before and after passive infusion of bNAbs 3BNC117 and/or 10-1074 in twelve participants from four ATI trials[1-4], including seven post-intervention controllers (PICs) and five post-intervention non-controllers (PINCs; Fig. 1a, Table 1). We synthesized peptides matching class I HLA-optimal HIV epitopes encoded by autologous intact proviral DNA sequenced from each participant[27] (Supplementary Data 1) and mapped epitope-specific CD8⁺ T cell responses by interferon-γ enzyme-linked immunospot (IFN-γ ELISpot, Fig. 1b). A mean of 3.5 (range 1-8) HIV epitope-specific CD8⁺ T cell responses per participant was identified, and neither response breadth, induction of new responses against HLA-optimal HIV epitopes reported to be presented by the expressed HLA class I alleles, nor magnitude of IFN-γ production was associated with PIC (Fig. 1c,d, Supplementary Data 1). These data indicate that the induction of *de novo* CD8⁺ T cell responses against known HLA-optimal HIV epitopes following bNAb administration is not a unique correlate of PIC.

HIV-specific CD8⁺ T cell stemness precedes PIC

Because proliferation is better correlated with cytotoxic function and spontaneous control of HIV viremia than IFN-γ production[13,14,16-18], we next measured the ability of CD8⁺ T cells to proliferate upon stimulation with cognate HIV peptides corresponding to each response identified by IFN-γ ELISpot (Fig. 2a,b, Extended Data Fig. 1a). Pre-intervention proliferative capacity of CD8⁺ T cells against autologous HIV epitopes was on average more than tenfold higher in PICs relative to PINCs (mean 9.7% vs. 0.9%, median 3.6% vs. 0.3% CFSE-low, $p<0.001$, Fig. 2c). Notably, participant 314 had especially strong proliferative responses (range 16.0 – 49.7% CFSE-low) against 5 distinct epitopes (Fig. 2c) and was the only participant whose intact HIV DNA reservoir was below the assay detection limit (Table 1), suggesting a potential role for highly functional HIV epitope-specific CD8⁺ T cells in limiting HIV persistence in this participant. Proliferative capacity

remained significantly higher in PICs than PINCs even when responses from this participant were excluded from analysis. Following bNAb administration, proliferative capacity of responses from both participant groups modestly but significantly increased (median 1.3-fold, $p<0.01$ PICs, $p<0.05$ PINCs, Fig. 2c) and remained significantly higher in PICs than PINCs following intervention (mean 10.6% vs. 1.3%, median 3.8% vs. 0.4% CFSE-low, $p<0.001$, Fig. 2c). This modest increase was consistent with previous observations attributed to a potential bNAb-induced vaccinal effect[5-9] but was not unique to participants who controlled viremia. Instead, control of viremia was associated with HIV-specific $CD8^+$ T cell proliferative capacity that was higher before and further enhanced following intervention.

To assess the ability of HIV epitope-specific $CD8^+$ T cells to mount cytotoxic recall responses against autologous $CD4^+$ T cells pulsed with cognate HIV peptides, we performed expanded antigen-specific elimination assays[28] on immunodominant responses from participants with sufficient specimen availability (Fig. 2d,e, Extended Data Fig. 1b). Recall cytotoxicity was strongly associated with proliferative capacity (Spearman $\rho=0.80$, $p<0.0001$, Fig. 2f), consistent with prior data from spontaneous HIV controllers[17,18,28] and further supporting a role for highly functional HIV-specific $CD8^+$ T cells in PIC.

To further characterize functional HIV-specific $CD8^+$ T cells in PIC, we next assessed their *ex vivo* phenotypes by measuring surface expression of differentiation markers on unstimulated peptide-HLA (pHLA) multimer-stained $CD8^+$ T cells (Fig. 2g, Extended Data Fig. 1c, Supplementary Data 1). HIV epitope-specific $CD8^+$ T cells in PICs had a higher proportion of $CD45RA^+CD62L^+$ stem cell-like memory (T_{SCM}, $p<0.05$, Fig. 2h) whereas those from PINCs had a higher proportion of $CD45RA^-CD62L^-$ effector-memory (T_{EM}) prior to intervention ($p<0.01$, Fig. 2i). In comparison, $CD8^+$ T cell responses to cytomegalovirus (CMV) or influenza virus had a higher proportion of $CD45RA^+CD62L^-$ terminally-differentiated T_{EMRA} cells (Extended Data Fig. 1d). The frequency of

T_{SCM} cells among HIV epitope-specific $CD8^+$ T cells in PICs modestly (median 1.2-fold) but significantly (p<0.01) increased among PICs following bNAb administration and remained significantly higher post-intervention than in PINCs (p<0.01, Fig. 2h). Moreover, T_{SCM} frequency was proportional to proliferative capacity (Spearman ρ=0.64, p<0.01, Fig. 2j). Together, these results implicate HIV epitope-specific $CD8^+$ T cell stemness in PIC.

Molecular signatures of $CD8^+$ T cell stemness in PIC

To determine molecular signatures underlying the superior functional capacity of HIV-specific $CD8^+$ T cells in PICs, we next assessed differential expression of genes and surface proteins among HIV and CMV epitope-specific $CD8^+$ T cells at single-cell resolution via CITE-seq analyses of 15,466 pHLA multimer-stained cells from PICs and PINCs (Fig. 3a, Supplementary Data 1). Multimodal clustering of all samples based upon differential gene expression and surface markers revealed eight clusters, which were manually annotated based upon differentially expressed genes, gene sets, and surface markers (Fig. 3b; Extended Data Figs. 2, 3a-b). Cluster 0 was elevated among HIV-specific cells in PINCs, whereas cluster 1 was comparable between groups and clusters 2-7 were elevated among HIV-specific cells in PICs (Fig. 3c). PINC-associated cluster 0 expressed canonical effector-memory (T_{EM}) and exhaustion (T_{EX}) markers including CD45RO, PD-1, TIGIT, and *TOX* (Fig. 3d), indicating a potential role for T cell exhaustion in decreased functionality of HIV-specific $CD8^+$ T cells among PINCs. In contrast, PIC-associated cluster 6 expressed canonical T_{SCM} genes and surface proteins associated with stemness, including CD45RA, CD62L, CCR7, CD27, and *TCF7* (Fig. 3d)[29], consistent with our flow cytometric analyses (Fig. 2h-i). This T_{SCM}-like cluster exhibited low inhibitory receptor expression, elevated oxidative phosphorylation gene signatures, and increased surface expression of CD73 (Fig. 3d). T cells expressing CD73, an ectonucleotidase with previously reported roles in regulating metabolism via nicotinamide adenine dinucleotide modulation[30], have previously been associated with spontaneous HIV control and reduced exhaustion[31,32]. PIC was also associated

with T_{EM}-like cells expressing interferon response genes (cluster 5) and T_{SCM}-like cells co-expressing signatures of glycolysis that share features of transitory cells derived from stem-like precursors (cluster 4; Fig. 3d-g, Extended Data Fig. 2, Supplementary Data 2)[33]. Unlike T_{EX} cells, which express effector-like signatures but are impaired for glycolysis, oxidative phosphorylation, and proliferative potential[34], metabolic signatures elevated in T cells from PICs have been previously proposed to prime them for rapid signaling in response to antigen[35]. These data indicate HIV-specific $CD8^+$ T cells in PICs are characterized by molecular signatures of stemness, reduced exhaustion, and metabolic fitness.

Augmented stemness is associated with pre-existing clonotypes

We next investigated longitudinal changes following bNAb administration to define molecular signatures associated with the modest but significant augmentation of $CD8^+$ T cell stemness and proliferative capacity observed (Fig. 2c,i). As broadening of response specificities was not associated with PIC (Fig. 1c), we evaluated longitudinal changes within HIV epitope-specific responses targeted prior to intervention. PIC was not uniquely associated with diversification or expansion of T cell receptor (TCR) clonotypes following intervention (Fig. 4a, Supplementary Data 3). Epitope-specific responses were oligoclonal, with more than half of each response comprising one or two dominant clonotypes and without substantial emergence of new clonotypes following bNAb administration (Fig. 4b, Extended Data Fig. 3c,d).

By flow cytometry, we observed no significant increases in frequencies of HIV epitope-specific $CD8^+$ T cells (Fig. 4c), their activation measured by CD38 and HLA-DR co-expression (Fig. 4d), their *in vivo* proliferation marked by Ki67 expression (Fig. 4e), or their cytotoxic differentiation measured by perforin and granzyme B co-expression (Fig. 4f). These results indicate a lack of peripheral response to antigen at the time points studied, which preceded waning of bNAb concentrations to subtherapeutic levels and detectable HIV recrudescence. By multimodal single-

cell analyses, we observed modest but significant upregulation of both CD45RA and CD62L surface marker expression following bNAb administration, consistent with increases in T_{SCM} frequencies observed by flow cytometry (Fig. 2i), and an increase in gene signatures of oxidative metabolism (Fig. 4g-i, Supplementary Data 4), which has previously been associated with spontaneous control of HIV[36]. Following bNAb administration, we also observed small increases in the frequencies of T_{SCM} and $CD127^+CD73^+$ cell clusters, which have previously been associated with proliferative long-lived memory[37,38] and share gene signatures with follicular $CD8^+$ T cells in lymphoid tissues (Fig. 4j-k)[39]. Although pre-existing differences in stemness better distinguished PICs from PINCs than longitudinal changes (Fig. 2c, 3d, 4j), our results suggest that augmentation of $CD8^+$ T cell stemness in peripheral circulation following bNAb administration may involve $CD8^+$ T cell recirculation from lymphoid tissue sites of early bNAb-suppressed virus re-emergence, consistent with previous results in non-human primates[6].

Discussion

In this study, we explored HIV-specific $CD8^+$ T cell responses in PWH on ART who received bNAbs and underwent concurrent or subsequent ATI. Examination of PICs who have remained mostly aviremic without ART for up to 7 years from four similar interventional trials enabled us to investigate immune correlates of durable PIC at greater sensitivity than was feasible from individual trials. By evaluating cellular immunity at epitope-specific resolution using reagents matching autologous virus, our study additionally avoided potential confounding effects of immune escape. Our results indicate that HIV-specific $CD8^+$ T cells are more functional both prior to and following intervention in people who subsequently control viremia without ART relative to those who receive the same intervention but experience viral rebound. HIV-specific $CD8^+$ T cells in PICs were characterized by molecular and functional hallmarks of stemness, including the ability to proliferate, differentiate, and mount cytotoxic recall responses against HIV antigens matched to autologous virus.

CD8+ T cell stemness has been previously associated with spontaneous control of HIV viremia, but its role in control of viremia following treatment interruption is not well established. Class I HLA alleles associated with spontaneous HIV control do not appear to be associated with PTC[19,22,40]. Although HIV-specific CD8+ T cell responses are dysfunctional in the majority of PWH and their functionality is not typically restored by ART[41], CD8+ T cell functionality has been associated with case reports of PTC[42,43], and preservation of HIV-specific CD8+ T cell functionality[44,45] may contribute to higher rates of PTC observed among early-treated PWH[19,20]. In addition, enhanced CD8+ T cell functionality and stemness in some individuals following prolonged ART[46,47] may also contribute to PTC in PWH treated during chronic infection. However, as CD8+ T cell responses to recrudescent viremia typically lag HIV replication, they are likely insufficient to prevent rebound viremia in most noninterventional ATI settings. Consistent with this, CD8+ T cell responses are not associated with time-to-rebound but rather are associated with setpoint viral loads[48]. As ART is re-initiated upon viral rebound in most ATI trials, the impact of CD8+ T cells on viral load setpoint is not typically measured and PTC in noninterventional studies has more frequently been associated with autologous neutralization and innate immunity[22,23,40].

As HIV frequently escapes from autologous neutralizing antibodies, passive infusion of exogenous bNAbs, especially in combination, has enabled prolonged suppression of viremia[2,49,50]. CD8+ T cells have been implicated in durable PIC among bNAb recipients due to a proposed vaccinal effect by which antigen-antibody complexes lead to the stimulation of cellular immunity[1-9]. While modest augmentation of CD8+ T cell proliferative capacity following bNAb administration was consistently observed in our study, this effect was neither unique to PIC nor associated with new responses or TCR clonotypes against known HLA-optimal epitopes. Instead, our results implicate precise features of HIV-specific CD8+ T cells prior to intervention that are further enhanced by bNAb administration and are associated with subsequent PIC, including their

stemness, proliferative capacity, recall cytotoxicity, and metabolic fitness. Indeed, these features have previously been associated with superior HIV-specific $CD8^+$ T cell functionality in spontaneous HIV controllers[11,13,16-18,36], from whom $CD8^+$ T cells and exogenous bNAbs can synergize to elicit *in vitro* HIV suppression[51]. We hypothesize that by limiting the rate and magnitude of HIV recrudescence, bNAbs allow functional $CD8^+$ T cell responses a better chance to contain early virus rebound in lymphoid tissues, mediating PIC after bNAbs wane below therapeutic concentrations.

Despite including participants from four trials, our study remained limited by sample availability in multiple aspects, including scope and statistical power. As it was not feasible to screen $CD8^+$ T cell responses using overlapping peptides spanning the entire HIV-1 proteome, we focused on known HLA-optimal epitopes matching autologous provirus sequence to facilitate downstream analyses using pHLA multimers. It is possible that our approach may have missed responses against as-yet undefined epitopes or those below our detection limit. Due to limitations in specimen and pHLA multimer availability, we were able to profile only one-third of detected HIV-specific responses by cytometry and multiomics. As our study focused on HIV-specific $CD8^+$ T cell responses, we did not evaluate other immune parameters that may contribute to PIC. Sampling of peripheral blood at a single post-intervention time point limited our ability to observe *in vivo* proliferative and cytotoxic responses to recrudescent viremia. Due to the retrospective nature of our study, prospective studies will be required to determine the predictive capacity of HIV-specific $CD8^+$ T cell features preceding PIC. Studies investigating epitope-specific $CD8^+$ T cell responses in lymphoid tissues, the primary sites of HIV persistence and recrudescence[52,53], and measurement of additional immune parameters such as autologous neutralization, innate immunity, and HIV-specific $CD4^+$ T cell responses, will be important to further delineate mechanisms of PIC.

Ongoing trials aim to elicit PIC in a larger proportion of PWH via improved or combinatorial interventions, including long-acting bNAbs[54], therapeutic vaccination[55], and agonists of cytokines such as IL-15[56], which can rewire cellular metabolism of dysfunctional HIV-specific $CD8^+$ T cells[57] and promote their migration to B cell follicles in lymphoid tissues[58]. Complementary new data emerging from two independent interventional trials further support a role for $CD8^+$ T cell proliferation in PIC[55,59]. Our results suggest that immunotherapies capable of enhancing virus-specific $CD8^+$ T cell stemness, proliferative capacity, and recall cytotoxicity may dramatically enhance the ability to elicit durable HIV remission elicited by bNAb administration.

REFERENCES

1 Mendoza, P. *et al.* Combination therapy with anti-HIV-1 antibodies maintains viral suppression. *Nature* **561**, 479-484 (2018). https://doi.org/10.1038/s41586-018-0531-2

2 Gaebler, C. *et al.* Prolonged viral suppression with anti-HIV-1 antibody therapy. *Nature* **606**, 368-374 (2022). https://doi.org/10.1038/s41586-022-04597-1

3 Gunst, J. D. *et al.* Early intervention with 3BNC117 and romidepsin at antiretroviral treatment initiation in people with HIV-1: a phase 1b/2a, randomized trial. *Nat Med* **28**, 2424-2435 (2022). https://doi.org/10.1038/s41591-022-02023-7

4 Gunst, J. D. *et al.* Impact of a TLR9 agonist and broadly neutralizing antibodies on HIV-1 persistence: the randomized phase 2a TITAN trial. *Nat Med* **29**, 2547-2558 (2023). https://doi.org/10.1038/s41591-023-02547-6

5 Nishimura, Y. *et al.* Early antibody therapy can induce long-lasting immunity to SHIV. *Nature* **543**, 559-563 (2017). https://doi.org/10.1038/nature21435

6 Nishimura, Y. *et al.* Immunotherapy during the acute SHIV infection of macaques confers long-term suppression of viremia. *J Exp Med* **218** (2021). https://doi.org/10.1084/jem.20201214

7 Lim, S. Y. *et al.* Induction of durable remission by dual immunotherapy in SHIV-infected ART-suppressed macaques. *Science* **383**, 1104-1111 (2024). https://doi.org/10.1126/science.adf7966

8 Niessl, J. *et al.* Combination anti-HIV-1 antibody therapy is associated with increased virus-specific T cell immunity. *Nat Med* **26**, 222-227 (2020). https://doi.org/10.1038/s41591-019-0747-1

9 Rosas-Umbert, M. *et al.* Administration of broadly neutralizing anti-HIV-1 antibodies at ART initiation maintains long-term CD8(+) T cell immunity. *Nat Commun* **13**, 6473 (2022). https://doi.org/10.1038/s41467-022-34171-2

10 Landovitz, R. J., Scott, H. & Deeks, S. G. Prevention, treatment and cure of HIV infection. *Nat Rev Microbiol* **21**, 657-670 (2023). https://doi.org/10.1038/s41579-023-00914-1

11 Collins, D. R., Gaiha, G. D. & Walker, B. D. CD8(+) T cells in HIV control, cure and prevention. *Nat Rev Immunol* **20**, 471-482 (2020). https://doi.org/10.1038/s41577-020-0274-9
12 Li, J. Z. & Blankson, J. N. How elite controllers and posttreatment controllers inform our search for an HIV-1 cure. *J Clin Invest* **131** (2021). https://doi.org/10.1172/JCI149414
13 Migueles, S. A. *et al.* HIV-specific CD8+ T cell proliferation is coupled to perforin expression and is maintained in nonprogressors. *Nat Immunol* **3**, 1061-1068 (2002). https://doi.org/10.1038/ni845
14 Horton, H. *et al.* Preservation of T cell proliferation restricted by protective HLA alleles is critical for immune control of HIV-1 infection. *J Immunol* **177**, 7406-7415 (2006). https://doi.org/10.4049/jimmunol.177.10.7406
15 Collins, D. R. *et al.* Cytolytic CD8(+) T cells infiltrate germinal centers to limit ongoing HIV replication in spontaneous controller lymph nodes. *Sci Immunol* **8**, eade5872 (2023). https://doi.org/10.1126/sciimmunol.ade5872
16 Rutishauser, R. L. *et al.* TCF-1 regulates HIV-specific CD8+ T cell expansion capacity. *JCI Insight* **6** (2021). https://doi.org/10.1172/jci.insight.136648
17 Migueles, S. A. *et al.* Lytic granule loading of CD8+ T cells is required for HIV-infected cell elimination associated with immune control. *Immunity* **29**, 1009-1021 (2008). https://doi.org/10.1016/j.immuni.2008.10.010
18 Collins, D. R. *et al.* Functional impairment of HIV-specific CD8(+) T cells precedes aborted spontaneous control of viremia. *Immunity* **54**, 2372-2384 e2377 (2021). https://doi.org/10.1016/j.immuni.2021.08.007
19 Saez-Cirion, A. *et al.* Post-treatment HIV-1 controllers with a long-term virological remission after the interruption of early initiated antiretroviral therapy ANRS VISCONTI Study. *PLoS Pathog* **9**, e1003211 (2013). https://doi.org/10.1371/journal.ppat.1003211
20 Namazi, G. *et al.* The Control of HIV After Antiretroviral Medication Pause (CHAMP) Study: Posttreatment Controllers Identified From 14 Clinical Studies. *J Infect Dis* **218**, 1954-1963 (2018). https://doi.org/10.1093/infdis/jiy479
21 Gunst, J. D. *et al.* Time to HIV viral rebound and frequency of post-treatment control after analytical interruption of antiretroviral therapy: an individual data-based meta-analysis of 24 prospective studies. *Nat Commun* **16**, 906 (2025). https://doi.org/10.1038/s41467-025-56116-1
22 Etemad, B. *et al.* HIV post-treatment controllers have distinct immunological and virological features. *Proc Natl Acad Sci U S A* **120**, e2218960120 (2023). https://doi.org/10.1073/pnas.2218960120
23 Esmaeilzadeh, E. *et al.* Autologous neutralizing antibodies increase with early antiretroviral therapy and shape HIV rebound after treatment interruption. *Sci Transl Med* **15**, eabq4490 (2023). https://doi.org/10.1126/scitranslmed.abq4490
24 Klastrup, V., Gunst, J. D., Rasmussen, T. A., Tolstrup, M. & Sogaard, O. S. Factors influencing virologic control during analytical treatment interruptions in HIV cure trials - a pooled analysis of individual level data. *J Infect Dis* (2025). https://doi.org/10.1093/infdis/jiaf163

25 Scheid, J. F. *et al.* HIV-1 antibody 3BNC117 suppresses viral rebound in humans during treatment interruption. *Nature* **535**, 556-560 (2016). https://doi.org/10.1038/nature18929
26 Sandel, D. A., Rutishauser, R. L. & Peluso, M. J. Post-intervention control in HIV immunotherapy trials. *Curr Opin HIV AIDS* **20**, 70-79 (2025). https://doi.org/10.1097/COH.0000000000000890
27 Lu, C. L. *et al.* Relationship between intact HIV-1 proviruses in circulating CD4(+) T cells and rebound viruses emerging during treatment interruption. *Proc Natl Acad Sci U S A* **115**, E11341-E11348 (2018). https://doi.org/10.1073/pnas.1813512115
28 Collins, D. R. *et al.* Expanded Antigen-Specific Elimination Assay to Measure Human CD8(+) T Cell Cytolytic Potential. *Curr Protoc* **4**, e1109 (2024). https://doi.org/10.1002/cpz1.1109
29 Fuertes Marraco, S. A. *et al.* Long-lasting stem cell-like memory CD8+ T cells with a naive-like profile upon yellow fever vaccination. *Sci Transl Med* **7**, 282ra248 (2015). https://doi.org/10.1126/scitranslmed.aaa3700
30 Zhan, J. *et al.* Regulation of CD73 on NAD metabolism: Unravelling the interplay between tumour immunity and tumour metabolism. *Cell Commun Signal* **22**, 387 (2024). https://doi.org/10.1186/s12964-024-01755-y
31 Carriere, M. *et al.* HIV "elite controllers" are characterized by a high frequency of memory CD8+ CD73+ T cells involved in the antigen-specific CD8+ T-cell response. *J Infect Dis* **209**, 1321-1330 (2014). https://doi.org/10.1093/infdis/jit643
32 Toth, I. *et al.* Decreased frequency of CD73+CD8+ T cells of HIV-infected patients correlates with immune activation and T cell exhaustion. *J Leukoc Biol* **94**, 551-561 (2013). https://doi.org/10.1189/jlb.0113018
33 Hudson, W. H. *et al.* Proliferating Transitory T Cells with an Effector-like Transcriptional Signature Emerge from PD-1(+) Stem-like CD8(+) T Cells during Chronic Infection. *Immunity* **51**, 1043-1058 e1044 (2019). https://doi.org/10.1016/j.immuni.2019.11.002
34 Bengsch, B. *et al.* Bioenergetic Insufficiencies Due to Metabolic Alterations Regulated by the Inhibitory Receptor PD-1 Are an Early Driver of CD8(+) T Cell Exhaustion. *Immunity* **45**, 358-373 (2016). https://doi.org/10.1016/j.immuni.2016.07.008
35 Shyer, J. A., Flavell, R. A. & Bailis, W. Metabolic signaling in T cells. *Cell Res* **30**, 649-659 (2020). https://doi.org/10.1038/s41422-020-0379-5
36 Angin, M. *et al.* Metabolic plasticity of HIV-specific CD8(+) T cells is associated with enhanced antiviral potential and natural control of HIV-1 infection. *Nat Metab* **1**, 704-716 (2019). https://doi.org/10.1038/s42255-019-0081-4
37 Boettler, T. *et al.* Expression of the interleukin-7 receptor alpha chain (CD127) on virus-specific CD8+ T cells identifies functionally and phenotypically defined memory T cells during acute resolving hepatitis B virus infection. *J Virol* **80**, 3532-3540 (2006). https://doi.org/10.1128/JVI.80.7.3532-3540.2006
38 Fang, F. *et al.* The cell-surface 5'-nucleotidase CD73 defines a functional T memory cell subset that declines with age. *Cell Rep* **37**, 109981 (2021). https://doi.org/10.1016/j.celrep.2021.109981

39 Leong, Y. A. *et al.* CXCR5(+) follicular cytotoxic T cells control viral infection in B cell follicles. *Nat Immunol* **17**, 1187-1196 (2016). https://doi.org/10.1038/ni.3543
40 Essat, A. *et al.* A genetic fingerprint associated with durable HIV remission after interruption of antiretroviral treatment: ANRS VISCONTI/PRIMO. *Med*, 100670 (2025). https://doi.org/10.1016/j.medj.2025.100670
41 Migueles, S. A. *et al.* Defective human immunodeficiency virus-specific CD8+ T-cell polyfunctionality, proliferation, and cytotoxicity are not restored by antiretroviral therapy. *J Virol* **83**, 11876-11889 (2009). https://doi.org/10.1128/JVI.01153-09
42 Veenhuis, R. T. *et al.* Long-term remission despite clonal expansion of replication-competent HIV-1 isolates. *JCI Insight* **3** (2018). https://doi.org/10.1172/jci.insight.122795
43 Blazkova, J. *et al.* Distinct mechanisms of long-term virologic control in two HIV-infected individuals after treatment interruption of anti-retroviral therapy. *Nat Med* **27**, 1893-1898 (2021). https://doi.org/10.1038/s41591-021-01503-6
44 Ndhlovu, Z. M. *et al.* Augmentation of HIV-specific T cell function by immediate treatment of hyperacute HIV-1 infection. *Sci Transl Med* **11** (2019). https://doi.org/10.1126/scitranslmed.aau0528
45 Takata, H. *et al.* Long-term antiretroviral therapy initiated in acute HIV infection prevents residual dysfunction of HIV-specific CD8(+) T cells. *EBioMedicine* **84**, 104253 (2022). https://doi.org/10.1016/j.ebiom.2022.104253
46 White, E. *et al.* Clonal succession after prolonged antiretroviral therapy rejuvenates CD8(+) T cell responses against HIV-1. *Nat Immunol* **25**, 1555-1564 (2024). https://doi.org/10.1038/s41590-024-01931-9
47 Vigano, S. *et al.* Prolonged Antiretroviral Therapy Preserves HIV-1-Specific CD8 T Cells with Stem Cell-Like Properties. *J Virol* **89**, 7829-7840 (2015). https://doi.org/10.1128/JVI.00789-15
48 Okoye, A. A. *et al.* CD8+ T cells fail to limit SIV reactivation following ART withdrawal until after viral amplification. *J Clin Invest* **131** (2021). https://doi.org/10.1172/JCI141677
49 Sneller, M. C. *et al.* Combination anti-HIV antibodies provide sustained virological suppression. *Nature* **606**, 375-381 (2022). https://doi.org/10.1038/s41586-022-04797-9
50 Julg, B. *et al.* Safety and antiviral effect of a triple combination of HIV-1 broadly neutralizing antibodies: a phase 1/2a trial. *Nat Med* **30**, 3534-3543 (2024). https://doi.org/10.1038/s41591-024-03247-5
51 Veenhuis, R. T., Garliss, C. C., Bailey, J. R. & Blankson, J. N. CD8 Effector T Cells Function Synergistically With Broadly Neutralizing Antibodies to Enhance Suppression of HIV Infection. *Front Immunol* **12**, 708355 (2021). https://doi.org/10.3389/fimmu.2021.708355
52 Boritz, E. A. *et al.* Multiple Origins of Virus Persistence during Natural Control of HIV Infection. *Cell* **166**, 1004-1015 (2016). https://doi.org/10.1016/j.cell.2016.06.039
53 Estes, J. D. *et al.* Defining total-body AIDS-virus burden with implications for curative strategies. *Nat Med* **23**, 1271-1276 (2017). https://doi.org/10.1038/nm.4411

54 Lee, M. J. *et al.* The RIO trial: rationale, design, and the role of community involvement in a randomised placebo-controlled trial of antiretroviral therapy plus dual long-acting HIV-specific broadly neutralising antibodies (bNAbs) in participants diagnosed with recent HIV infection-study protocol for a two-stage randomised phase II trial. *Trials* **23**, 263 (2022). https://doi.org/10.1186/s13063-022-06151-w

55 Peluso, M. *et al.* Combination immunotherapy induces post-intervention control of HIV. *Research Square* (2025). https://doi.org/https://doi.org/10.21203/rs.3.rs-6141479/v1

56 Nel, C. & Frater, J. Enhancing broadly neutralising antibody suppression of HIV by immune modulation and vaccination. *Front Immunol* **15**, 1478703 (2024). https://doi.org/10.3389/fimmu.2024.1478703

57 Perdomo-Celis, F. *et al.* Reprogramming dysfunctional CD8+ T cells to promote properties associated with natural HIV control. *J Clin Invest* **132** (2022). https://doi.org/10.1172/JCI157549

58 Webb, G. M. *et al.* The human IL-15 superagonist N-803 promotes migration of virus-specific CD8+ T and NK cells to B cell follicles but does not reverse latency in ART-suppressed, SHIV-infected macaques. *PLoS Pathog* **16**, e1008339 (2020). https://doi.org/10.1371/journal.ppat.1008339

59 Altaf, M. *et al.* Sustained T-Cell Mediated Immunity After LS-bNAbs in the RIO Trial: A Vaccinal Effect. *Topics in Antiviral Medicine* **33**, 506 (2025).

TABLES

PID	Study	Intervention	Phenotype	Samples	Age	Sex	Race	HIV/ART Duration	CD4 Count	Intact HIV DNA	HLA	HIV Epitopes
9243 ▼	MCA-906	3x 3BNC117+ 10-1074 during ATI	PINC	ATI start; 12w post-ATI	29	M	AI, H	5y/5y	583	0.17	A24,30 B15,31 C02,15	49 A
9252 ▲	MCA-906	3x 3BNC117+ 10-1074 during ATI	PINC	ATI start; 12w post-ATI	51	F	B	11y/11y	598	1.71	A02,66 B39,78 C12,16	37 A
9254 ♦	MCA-906	3x 3BNC117+ 10-1074 during ATI	PIC	ATI start; 12w post-ATI	48	M	W	21y/21y	860	NA	A01,29 B38,44 C12,16	22 A
9255 ▲	MCA-906	3x 3BNC117+ 10-1074 during ATI	PIC	ATI start; 12w post-ATI	30	M	W	5y/4y	1360	1.89	A03,25 B18,44 C07,12	41 A
5106 ■	MCA-965	7x 3BNC117+ 10-1074 during ATI	PIC	ATI start; 12w post-ATI	31	M	B	6y/6y	671	7.3	A03,03 B18,57 C12,18	61 A
5111 ■	MCA-965	7x 3BNC117+ 10-1074 during ATI	PINC	ATI start; 12w post-ATI	55	M	W	20y/16y	760	2.5	A11,32 B35,44 C05,12	38 A
5114 ●	MCA-965	7x 3BNC117+ 10-1074 during ATI	PINC	ATI start; 12w post-ATI	54	M	B	15y/15y	545	6.1	A03,68 B07,15 C07,07	53 A
5120 ●	MCA-965	7x 3BNC117+ 10-1074 during ATI	PIC	ATI start; 12w post-ATI	50	M	W	19y/19y	1189	0.8	A02,29 B14,44 C01,03	42 A
107 ○	eCLEAR	2x 3BNC117+ 3xRMD at ART initiation	PIC	post-bNAb (pre-ATI)	45	M	W	1.2y/1y	650	50.2	A02,25 B15,44 C03,05	43 A
109 ♦	TITAN	2x 3BNC117+ 10-1074 during ATI	PINC	ATI start; 6w post-ATI	57	M	W	5y/5y	1250	93.5	A02,02 B07,51 C04,07	53 C
142 ★	TITAN	2x 3BNC117+ 10-1074 during ATI	PIC	ATI start; 6w post-ATI	57	M	W	5y/5y	1210	220.2	A01,02 B08,44 C05,07	48 A
314 ▼	TITAN	2x 3BNC117+ 10-1074 during ATI	PIC	ATI start; 6w post-ATI	55	F	W	2y/2y	1030	<1.2	A30,32 B13,51 C06,14	31 C

Table 1: Participant clinical and demographic characteristics. Participant ID (PID) and key for symbol-color combinations used to represent data from each participant; parent study; intervention (RMD, romidepsin); phenotype (PIC, post-intervention controller; PINC, post-intervention noncontroller); longitudinal sampling; age (years; NR, not reported); biological sex (M, male; F, female); race and ethnicity (AI, American Indian; B, Black; H, Hispanic; W, White); duration of HIV infection and ART before ATI (y, years); pre-intervention CD4 count (cells/μm^3 peripheral blood); intact HIV per 10^6 PBMCs reported previously as measured by Q^2VOA (IUPM, MCA-906[1]), Q4PCR (MCA-965[2]), or IPDA (eCLEAR[3], TITAN[4]); class I HLA alleles (protective alleles underlined); and total number of HLA-optimal HIV epitopes screened (A, autologous; C,

clade B consensus). Plasma viral loads were undetectable (<20 HIV RNA copies/ml) at all sample time points. NA, not available.

FIGURE LEGENDS

Fig. 1: Autologous HIV epitope-specific CD8⁺ T cell responses in post-intervention controllers. (**a**) Study cohort overview. Longitudinal PBMCs were included from 7 post-intervention controller (PIC) and 5 post-intervention noncontroller (PINC) participants pre- and post-infusion of bNAbs 3BNC117 and 10-1074 from the MCA-906, MCA-965, TITAN and eCLEAR trials. Representative diagrams were modified from Mendoza *et al.*[1] with permission. (**b**) Schematic overview of autologous HIV-specific CD8⁺ T cell response mapping and representative interferon-γ (IFN-γ) ELISpot results. (**c-d**) Summary of longitudinal and between-group differences in breadth (c, *n*=6, 7, 5, 5 samples) and magnitude (d, *n*=23, 26, 22, 22 responses) of HIV epitope-specific responses. Center lines represent medians, ticks represent means, boxes represent first and third quartiles, and whiskers represent ranges. Color-symbol combinations represent participants (key in Table 1). *P*-values reported above plots from two-sided paired (longitudinal) or unpaired (between-group) *t*-tests.

Fig. 2: HIV-specific CD8⁺ T cell stemness precedes post-intervention control. (**a-b**) Schematic overview of HIV-specific CD8⁺ T cell proliferation assay (a) and representative longitudinal epitope-specific proliferation from one PIC (PID 5120) and one PINC (PID 9243; b). (**c**) Summary of longitudinal and between-group differences in proliferative capacity of CD8⁺ T cell responses against each autologous HIV-1 epitope for which responses were detected by IFN-γ ELISpot. Each data point represents the mean of triplicate wells for each response (*n*=23, 26, 22, 22 responses). (**d-e**) Schematic overview of expanded antigen-specific elimination assay to measure recall cytotoxicity (d) and representative results at increasing effector:target (E:T) ratios from one PIC (PID 142; blue) and one PINC (PID 109; red), including area under the curve (AUC)

summaries (e). (**f**) Correlation of proliferation and recall cytotoxicity, as measured in d-e, across responses from both pre- and post-intervention samples in PICs (blue) and PINCs (red). Correlation (ρ) and *p*-values calculated by Spearman correlation (*n*=41 responses). (**g**) Representative flow cytometric staining of memory subset markers CD45RA and CD62L on HIV peptide-HLA (pHLA) tetramer$^+$ CD8$^+$ T cells. (**h-i**) Summary of longitudinal and between-group differences in stem cell-like memory (T_{SCM}, h) and effector-memory (T_{EM}, i) subset frequencies among HIV pHLA tetramer$^+$ (Tet$^+$) CD8$^+$ T cell responses from PICs (*n*=9) and PINCs (*n*=7), and among CMV/flu Tet$^+$ CD8$^+$ T cells from both groups (*n*=8). (**j**) Correlation (ρ) and *p*-values calculated by Spearman correlation between proliferative capacity and percent T_{SCM} among Tet$^+$ CD8$^+$ T cells in PICs (blue) and PINCs (red), *n* = 16 responses. Center lines represent medians, boxes represent first and third quartiles, and whiskers represent ranges. Color-symbol combinations represent participants (key in Table 1). *P*-values reported above plots from two-sided Wilcoxon signed rank (between-group) or matched-pairs signed rank (longitudinal) tests (c), two-sided unpaired (between-group) or paired (longitudinal) *t*-tests (h-i), or Spearman correlation tests (f, j).

Fig. 3: Molecular signatures associated with post-intervention control. (**a**) Schematic overview of processing, isolation, and multiomics sequencing of HIV and CMV epitope-specific CD8$^+$ T cells. (**b**) Multimodal clustering by weighted nearest-neighbors plotted using uniform manifold approximation and projection (UMAP) for dimension reduction. (**c**) Cluster frequencies among HIV-specific CD8$^+$ T cells from both pre- and post-intervention samples in PICs and PINCs and among CMV-specific CD8$^+$ T cells and with cluster annotations based on differential expression of genes, gene sets, and surface markers shown in d (left); Breakdown of participant phenotype (PIC, PINC) and pathogen specificities (HIV, CMV) on UMAP plot as shown in b (right). *P*-values reported above plots from χ^2 tests. (**d**) Bubble plot comparing z-scaled mean normalized expression and detection rates for curated surface markers, transcripts (italics), and gene

signatures supporting cluster annotations, as detailed in Methods. (**e-f**) Volcano plots summarizing differentially expressed genes (e) and surface proteins (f) among HIV-specific $CD8^+$ T cells from PICs (blue) and PINCs (red). (**g**) Summary of top ten most significantly upregulated and downregulated gene set subnets from GSNA of HIV-specific $CD8^+$ T cells from PICs versus PINCs.

Fig. 4: Augmented $CD8^+$ T cell stemness following bNAb administration is associated with pre-existing clonotypes. (**a**) Longitudinal T-cell receptor (TCR) clonal diversification summarized as one minus Morisita-Horn Similarity Index (MHSI) among HIV-specific responses from PICs (blue, *n*=6) and PINCs (red, *n*=7) or CMV-specific responses (violet, *n*=4). (**b**) Longitudinal TCRβ CDR3 clonotypic frequencies and MHSI of HIV (*n*=13) and CMV (*n*=4) epitope-specific $CD8^+$ T cell responses (paired columns) at pre- and post-bNAb time points from sorted pHLA $tetramer^+$ cells, ordered and colored by within-response rank for all responses with ≥10 cells and longitudinal sampling and all clonotypes that occurred more than once in the data set; full data in Supplementary Data 3. (**c-f**) Summaries of epitope-specific frequencies measured by pHLA tetramer (tet) staining among total $CD8^+$ T cells (c), activation measured by surface CD38 and HLA-DR co-expression (d), proliferation measured by intranuclear Ki-67 (e), and cytotoxic effector differentiation measured by intracellular perforin and granzyme B co-expression (f) among HIV pHLA tet^+ $CD8^+$ T cell responses from PICs (*n*=9) and PINCs (*n*=7), and among CMV/flu tet^+ $CD8^+$ T cell responses (*n*=8). (**g-h**) Volcano plots summarizing longitudinal changes among HIV-specific $CD8^+$ T cell responses from all participants with longitudinal sampling in gene (g) and surface protein (h) expression before (pre, gold) and after (post, magenta) intervention. (**i**) Summary of top ten most significantly upregulated and downregulated gene set subnets from GSNA among HIV-specific $CD8^+$ T cells from post- versus pre-intervention. **(j)** Longitudinal cluster frequencies among HIV- and CMV-specific $CD8^+$ T cells from PIC and PINC. **(k)** Violin plot of single-cell AUCell expression levels of a gene signature associated with lymph node follicular

CD8+ T cells[39] across clusters. Center lines represent medians, boxes first and third quartiles, and whiskers ranges. Color-symbol combinations represent participants (key in Table 1). *P*-values reported above plots from two-sided Wilcoxon signed rank (a,k), two-sided paired (longitudinal) or unpaired (between-group) *t*-tests (b-e), χ^2 tests (j).

METHODS

Study participants

We obtained approximately 40-80 million cryopreserved PBMCs from participants of the previously reported MCA-906 (NCT02825797), MCA-965 (NCT03526848), eCLEAR (NCT03041012), and TITAN (NCT03837756) trials[1-4], including 7 PICs who maintained undetectable or very low plasma viral loads for more than 30 weeks (up to seven years, and in some cases still ongoing) and 5 PINCs who experienced rebound viremia following investigational infusion of bNAbs 3BNC-117 and/or 10-1074 (Table 1). Longitudinal samples were included for 11 of 12 participants based on specimen availability at time points immediately preceding (pre) or 6-12 weeks following (post) bNAb administration in the context of ATI. eCLEAR participant 107, from whom we only included a post-intervention sample, was excluded from all pre-intervention and longitudinal analyses and its inclusion/exclusion did not impact our conclusions. To avoid potentially confounding effects of viremia, samples were selected such that viremia was undetectable in all participants at the time points sampled, with rebound viremia in PINCs occurring several weeks after collection of the post-intervention samples evaluated. Secondary use of biological specimens was approved by the Mass General Brigham Human Research Committee following informed consent obtained during the primary studies in accordance with all applicable regulations and guidelines.

Peptides

Peptides matching autologous, HLA class I-optimal HIV epitopes were synthesized to a purity of at least 80% at the Mass General Brigham Peptide Research Core using automated solid-phase Fmoc/tBu chemistry followed by HPLC and MALDI-MS analysis[60].

Autologous HIV epitope-specific CD8⁺ T cell mapping

Cryopreserved PBMCs were thawed at 37°C, recovered in RPMI media (Sigma-Aldrich) supplemented with 10% fetal bovine serum (FBS, Sigma), 10 mM HEPES, 100 U/ml penicillin, 100 µg/mL streptomycin, and 292 µg/mL L-glutamine (Fisher Scientific; R10) overnight, resuspended at $1x10^6$ cells/mL in R10, and plated at 200 µL per well in Immobilon-P 96-well microtiter plates (Millipore) pre-coated with 2 µg/mL anti-IFN-γ (clone DK1, Mabtech). Individual HLA-optimal HIV-1 peptides matched to each subject's *HLA* genotype and autologous provirus sequence[27], where available, or for Clade B consensus sequence where unavailable (Supplementary Data 1), were added at 1 µM and incubated at 37°C overnight. Triplicate negative control wells did not receive peptide and positive control wells were treated with 1 µg/ml anti-CD3 (clone OKT3, Biolegend) and 1 µg/ml anti-CD28 (clone CD28.8, Biolegend) antibodies. ELISpot assays were performed following manufacturer's protocol via biotinylated anti-IFN-γ (clone B6-1, Mabtech) detection, streptavidin-ALP (Mabtech) and AP-conjugated substrate (BioRad) followed by disinfection with 0.05% Tween-20 (Thermo Fisher) and analysis using CTL ImmunoSpot Analyzer Pro version 7.0.38.16. Responses greater than 10 spots per well (50 spots per 10^6 PBMCs) and 3-fold above negative controls were scored as positive.

Proliferation

Cryopreserved PBMCs were thawed at 37°C, recovered in R10 media overnight, then stained at 37°C for 20 minutes with 0.5 µM CellTrace CFSE (Thermo Fisher) as per manufacturer's protocol. Cells were then quenched and washed twice with R10 media, resuspended at $1x10^6$ cells/mL in R10, and plated at 200 µL per well in 96-well round-bottom polystyrene plates (Corning). Individual

HLA-optimal HIV-1 peptides matching each response previously detected by IFN-γ ELISpot were added at 1 μM to triplicate wells and incubated at 37°C for 6 days before flow cytometric assessment. Triplicate negative control wells did not receive peptide and positive control wells received 1 μg/ml anti-CD3 (clone OKT3, Biolegend) and 1 μg/ml anti-CD28 (clone CD28.8, Biolegend) antibodies. On day 6, cells were stained using Live/Dead Violet viability dye (Thermo Fisher, 10^{-3} dilution), AlexaFluor700-anti-CD3 (clone SK7, Biolegend, 10^{-2} dilution), and APC-anti-CD8 (clone RPA-T8, Biolegend, 10^{-2} dilution), then analyzed by flow cytometry. Reported values for each epitope-specific response represent means of background-subtracted triplicates.

Recall cytotoxicity

Recall cytotoxicity of HIV-1 epitope-specific memory $CD8^+$ T cell responses was measured using the expanded antigen-specific elimination assay (EASEA) as per our published protocol[28]. Briefly, PBMCs were rested overnight in R10 then incubated with 100 ng/ml individual HLA-optimal HIV-1 peptide for six days to expand antigen-specific effector cells. Target $CD4^+$ T cells were isolated from PBMC by negative magnetic separation (StemCell Technologies), activated in 24-well non-treated polystyrene plates (Corning) pre-coated with 2 mg/ml anti-CD3 (clone OKT3, Biolegend) at 1-2 million cells/ml in R10 with 2 mg/ml anti-CD28 (clone CD28.2, Biolegend) and 50 U/ml IL-2 (Peprotech) at 37°C overnight, then expanded in tissue culture-treated 24-well plates (Corning) at 2 million cells/ml in R10 with 50 U/mL IL-2 at 37°C for five days. 50% of target cells were pulsed for 30 minutes at 37°C with 10 μM peptide and labeled with CellTrace Far Red dye (Thermo Fisher, 10^{-3} dilution) and mixed with unpulsed target cells 1:1, then labeled with CellTrace Violet dye (Thermo Fisher, 10^{-3} dilution). After six days of expansion, CFSE-labeled effector CD8+ T cells were isolated from pooled mononuclear cells by negative magnetic separation (StemCell Technologies) and co-cultured with target cells at effector:target (E:T) ratios of 0:1, 1:1, 2:1, 4:1, and 8:1 with 50,000 target cells/well in a treated 96-well polystyrene plate (Corning) for 4 hours. Effector-only populations were stained with APC-conjugated pHLA tetramers (1:50 dilution) and

all samples were stained with BV605-anti-CD3 (clone UCHT1, Biolegend, 10^{-2} dilution), BUV395-anti-CD8 (clone RPA-T8, BD Biosciences, 10^{-2} dilution), BV711-anti-CD4 (clone RPA-T4, Biolegend, 10^{-2} dilution) and Live/Dead Near-IR (Thermo Fisher, 10^{-3} dilution) then analyzed by flow cytometry. Results were gated as described previously and percent elimination and area-under-curve values were calculated as described previously[18,28].

Phenotypic cytometry

Peptide-HLA monomers for immunodominant responses (listed in Supplementary Data 1) were purchased from ImmunAware (Copenhagen, Denmark) as feasible. pHLA combinations were first validated for predicted binding using netMHCpan-4.0[61] and successful complex folding was experimentally validated by the manufacturer at the time of production. Tetramers were produced by multimerization with APC-conjugated streptavidin (Biolegend) as per manufacturer's protocol. Staining was performed using 4 nM individual APC-conjugated pHLA tetramers at 4°C for 30 minutes after 30-minute pre-treatment with 50 nM dasatinib to prevent *in vitro* cell activation and activation-induced cell death. Cells were then stained with Live/Dead Near-IR viability dye (Thermo Fisher, 10^{-3} dilution), RB705-anti-CD3 (clone UCHT1, BD Biosciences, 10^{-2} dilution), BV711-anti-CD8 (clone RPA-T8, Biolegend, 10^{-2} dilution), BUV395-anti-CD45RA (clone HI100, BD Biosciences, 10^{-2} dilution), RB780-anti-CD62L (clone DREG-56, BD Biosciences, 10^{-2} dilution), PE-Dazzle 594-anti-CD38 (clone HB7, Biolegend, 10^{-2} dilution), and BUV805-anti-HLA-DR (clone G46-6, BD Biosciences, 10^{-2} dilution) for 30 minutes at 4°C before fixation and permeabilization with eBiosciences Foxp3 transcription factor staining kit (Thermo) as per manufacturer's protocol, followed by intracellular staining for PE-anti-perforin (clone B-D48, Biolegend, 1:50 dilution), FITC-anti-granzyme B (clone GB11, Biolegend, 1:50 dilution), and intranuclear staining for BV421-anti-Ki-67 (clone Ki-67, Biolegend, 1:50 dilution). Data were acquired using a FACSSymphony A5 cytometer and FACSDiva version 9.2 (BD) and analyzed using FlowJo.

Single-cell multiomics

Cryopreserved PBMCs were thawed and rested overnight before negative-selection magnetic $CD8^+$ T cell isolation (StemCell Technologies), pre-treated for 30 minutes with 50 nM dasatinib (Selleck Chemicals), then stained with 4 nM APC, PE, or BV421-conjugated pHLA tetramers [prepared using Total-Seq C barcode-conjugated streptavidin (Biolegend) and pHLA monomers described and validated above (Immunaware), listed in Supplementary Data 1], Total-Seq C Human Universal Cocktail v2.0 (Biolegend) as per manufacturer's protocol, BV711-anti-CD8 (clone RPA-T8, Biolegend, 10^{-2} dilution) and unique Total-Seq C hashing antibodies (Biolegend, 1:200 dilution). $CD8^+$ T cells from an HLA-mismatched individual were included for estimation of nonspecific barcoded tetramer binding and sorting gates were set above this level. Cells were washed using a HT2000 laminar cell washer (Curiox) then resuspended in 2% FBS in PBS with Sytox Green viability dye (Thermo Fisher). Viable $pHLA^+$ $CD8^+$ T cells were isolated by fluorescence-activated cell sorting (FACS, counts in Supplementary Data 1) into a single pool then encapsulated after splitting across four GEM-wells using Chromium GEM-X (10X Genomics). Gene expression (GEX), surface protein expression (antibody-derived tags, ADT), and TCR (VDJ) libraries were generated using the 10X Chromium GEM-X Single Cell 5' v3 Dual Index kit with feature barcode technology (10X Genomics) following the manufacturer's protocol. Libraries were pooled at a 5:1:1 GEX:ADT:VDJ ratio and sequenced via paired-end reads on a NextSeq 2000 instrument with a 100-cycle P3 kit (Illumina).

Base-calling was performed using bcl2fastq and initial data-processing was performed using the Cell Ranger multi-analysis pipeline version 9.0.0 using refdata-gex-GRCh38-2020-A as a transcriptome reference and refdata-cellranger-vdj-GRCh38-alts-ensembl-5.0.0 as a VDJ reference. Gene expression (GEX), antibody capture (ADT), and TCR (VDJ) libraries were specified in the multi-analysis config file. Surface protein barcodes and hashtag barcodes

corresponding to samples were designated as “Antibody Capture” in the feature-reference file. After processing by Cell Ranger, the count matrix in sample_filtered_feature_bc_matrix was analyzed using Seurat version 5.3.0 in R version 4.3.1. Hashtag and pHLA specificity-level sample demultiplexing was performed using the HTOdemux() function of Seurat, and cells were removed for which HTO_classification.global was not "Singlet", hence removing cells with multiple or no hashtags. Cells for which pHLA barcodes were not detected were also removed, unless their corresponding TCR sequence matched expanded clones (>5 cells) from the data set, in which case they were reassigned to their matching specificity (1,757 total reassigned cells). 25,866 HIV-specific and CMV-specific cells were recovered, of which 15,466 passed filtering (Supplementary Data 1). The GEX library yielded 239 mean variable unique genes per cell, and 751 mean UMIs per cell. The ADT library yielded 522 mean UMIs per cell. To avoid clustering driven by clonotype-specific TCR gene expression, gene features for which the symbols matched the regular expression "^TR[ABDG][VJC]" were removed from the data set prior to clustering[62]. Using the Seurat function FindVariableFeatures(), 4,000 variable genes were selected for dimensionality reduction and differential expression analysis. Counts were log normalized, scaled and centered prior to dimensionality reduction and clustering. Clustering was performed using weighted nearest-neighbors (WNN) clustering via Seurat’s FindNeighbors() and FindClusters() functions with the argument resolution = 0.35.

Differential expression was performed using Seurat’s FindMarkers() function using default parameters, including Wilcoxon tests for statistical significance. Pathway analysis was performed using the tmodCERNOtest() from the tmod R package version 0.46.2[63] using a subset of MSigDB version v7.5.1[64] that included hallmark, gene ontology, reactome, KEGG, biocarta, and wikipathways gene sets. Primary cluster annotations as effector-memory (T_{EM}), central memory (T_{CM}), stem cell-like memory (T_{SCM}), and terminally differentiated memory (T_{EMRA}) were defined using CD45RA/RO and CD62L expression for comparability to flow cytometry results. Primary

and secondary cluster annotations were additionally supported by differentially expressed surface ADTs corresponding to CCR7, CD127, CD226, PD-1, TIGIT, CX3CR1, CD73; differentially expressed transcripts corresponding to *TCF7*, *TOX*, *GZMB*, *GZMK*, *GAPDH*, *ENO1, IFITM1*; and differentially expressed gene sets corresponding to aerobic glycolysis (WP4628), oxidative phosphorylation (M12919), interferon alpha response (M5911), lymph node follicular $CD8^+$ T cells (*CXCR5*, *SLAMF6*, *SELL*, *TCF7*, *ID3*, *CD200*, *ICOS*, *IL7R*, *BCL6*)[39], and T cell activation (M2810), which were quantified via AUCell[65] and plotted as bubble and/or violin plots in R. Gene set network analysis was performed using the GSNA R package, version 0.1.4.9, as previously described[15,18]. Longitudinal differential expression analyses were performed across HIV-specific responses from all participants with longitudinal sampling.

TCR clonotypes were assigned based on *TRB* CDR3 sequences and those appearing only once in the data set were excluded from clonotypic analysis. Diversity of clonotypes within a sample was quantified using Simpson diversity index and similarity of clonotypic composition between longitudinal samples was quantified using Morisita-Horn Similarity Index (MHSI)[66], whereas its inverse (1-MHSI) was used to assess longitudinal clonotypic divergence. MHSI measures overlap of clonotype proportions between two samples on a scale from 0 (no similarity) to 1 (identical) and is relatively robust to differences in sample size. Extended analyses are reported in Supplementary Data 3.

Statistical analyses, reproducibility, and figure preparation

Statistical analyses were performed using GraphPad Prism version 10.4 and R. Normality was estimated using Shapiro-Wilk tests. Normally distributed data were compared using *t*-tests and non-normally distributed data were compared using Wilcoxon signed rank tests and Spearman correlations. All replicate measurements reflect distinct biological samples or epitope-specific responses. All representative data shown is accompanied by summary data encompassing the

entire data set, with the precise number of biological replicates specified in each figure legend. All statistical tests were two-tailed. Wherever box-and-whisker diagrams are depicted, center lines represent medians, ticks represent means, boxes represent first and third quartiles, and whiskers represent ranges. Figures were prepared using Adobe Illustrator version 29.8.2, GraphPad Prism, R, and BioRender.com.

Data availability

Full single-cell multiomics data are available from the NCBI Gene Expression Omnibus (GEO: GSE294440). The GRCh38 reference genome is available from NCBI GenBank (GCA_000001405.15). MSigDB gene set references can be obtained from https://data.broadinstitute.org/gsea-msigdb/msigdb/release/7.5.1/. The remaining data are included within the manuscript and supplemental materials.

Reference Methods

60 Naranbhai, V. *et al.* T cell reactivity to the SARS-CoV-2 Omicron variant is preserved in most but not all individuals. *Cell* **185**, 1259 (2022). https://doi.org/10.1016/j.cell.2022.03.022

61 Jurtz, V. *et al.* NetMHCpan-4.0: Improved Peptide-MHC Class I Interaction Predictions Integrating Eluted Ligand and Peptide Binding Affinity Data. *J Immunol* **199**, 3360-3368 (2017). https://doi.org/10.4049/jimmunol.1700893

62 Sundell, T. *et al.* Single-cell RNA sequencing analyses: interference by the genes that encode the B-cell and T-cell receptors. *Brief Funct Genomics* **22**, 263-273 (2022). https://doi.org/10.1093/bfgp/elac044

63 Zyla, J. *et al.* Gene set enrichment for reproducible science: comparison of CERNO and eight other algorithms. *Bioinformatics* **35**, 5146-5154 (2019). https://doi.org/10.1093/bioinformatics/btz447

64 Subramanian, A. *et al.* Gene set enrichment analysis: a knowledge-based approach for interpreting genome-wide expression profiles. *Proc Natl Acad Sci U S A* **102**, 15545-15550 (2005). https://doi.org/10.1073/pnas.0506580102

65 Aibar, S. *et al.* SCENIC: single-cell regulatory network inference and clustering. *Nat Methods* **14**, 1083-1086 (2017). https://doi.org/10.1038/nmeth.4463

66 Horn, H. S. Measurement of "Overlap" in Comparative Ecological Studies. *The American Naturalist* **100**, 419-424 (1966).

Acknowledgements

The authors are grateful to the study participants; to eCLEAR, TITAN, MCA-906, and MCA-965 study clinicians and staff; and to Julia Hitschfel, Elif Çakan, James Chen, Rikke Olsen, and Giacomo Schmidt Frattari for helpful discussions and advice. This work was supported by funding from United States National Institutes of Health (AI184606, AI155233, AI152979, AI176579, AI44462), Howard Hughes Medical Institute, and the Lundbeck Foundation (R381–2021–1405). Funders had no role in study design, data collection and analysis, decision to publish or preparation of the manuscript.

Author contributions

DRC designed the study with input from BDW, MCN, OSS, MC, and JDG. MC, JDG, OSS, and MCN provided specimens. ZK, HW, MJO, DYC, and DRC performed experiments supported by technical contributions from JAA, APT, and NB and critical reagents from AK. JMU and DRC analyzed data. ML provided autologous provirus sequences. DRC and BDW supervised the work and obtained funding. DRC wrote the initial draft. All authors contributed to the final draft.

Competing interests

The authors declare no competing interests.

Supplementary Information

Supplementary information is available for this paper.

Correspondence and requests for materials should be addressed to David R. Collins.

EXTENDED DATA

Extended Data Fig. 1: Flow cytometric CD8⁺ T cell profiling. (**a-c**) Representative gating schema for measurement of epitope-specific proliferation (a), elimination of peptide-pulsed (CellTrace Far Red⁺) CD4⁺ T cell targets by peptide-expanded CD8⁺ T cell effectors (b), and phenotypic profiling of pHLA tetramer⁺ (Tet⁺) cells (c) by flow cytometry. Panel a also includes representative proliferation histogram overlays for HIV epitope-specific responses from PIC 5120 (blue) and PINC 9243 (red) relative to unstimulated controls (gray). (**d**) Memory subset frequencies among HIV Tet⁺ CD8⁺ T cell responses from PICs (*n*=9) and PINCs (*n*=7), and among CMV/flu Tet⁺ CD8⁺ T cell responses from both groups (*n*=8). Center lines represent medians, ticks represent means, boxes represent first and third quartiles, and whiskers represent ranges. Color-symbol combinations represent participants (key in Table 1). *P*-values reported above plots from two-sided paired (longitudinal) or unpaired (between-group) *t*-tests.

Extended Data Fig. 2: Differential expression between clusters. (a) Feature plots of expression levels of selected differentially expressed surface proteins and transcripts (italics) projected onto UMAP plots, supporting cluster annotations in Fig. 3. **(b)** Bubble plots of z-scaled mean normalized expression and detection rates for top differentially expressed transcripts (left) and surface proteins (right) upregulated in each cluster, ranked by adjusted *p* value.

Extended Data Fig. 3: Multimodal clustering and TCR clonotypes. (**a-d**) UMAP of HIV and CMV epitope-specific CD8⁺ T cells colored by WNN cluster (a), participant (b), *TRB* CDR3 clonotype (c), or *TRB* CDR3 clonotype separated by participant and response (d). Gray points represent singlets, whereas colored points are clonally expanded.

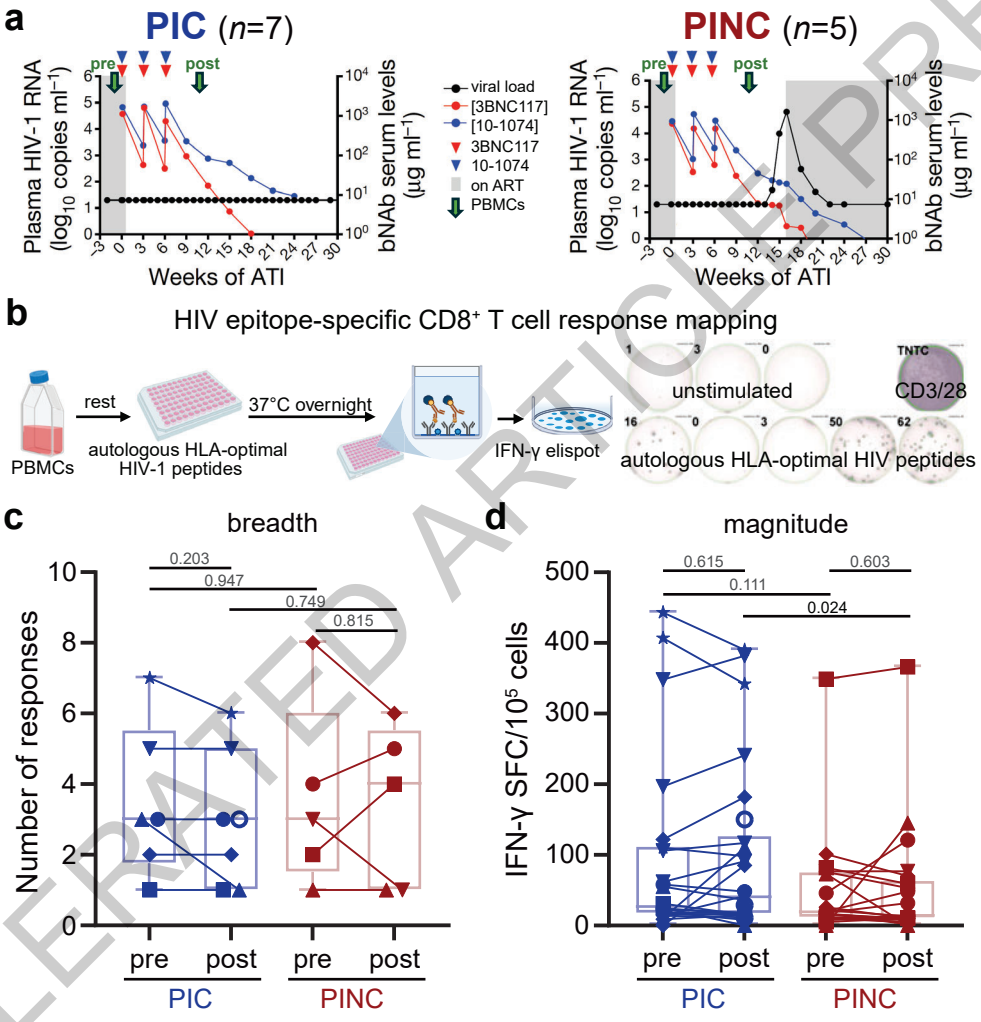

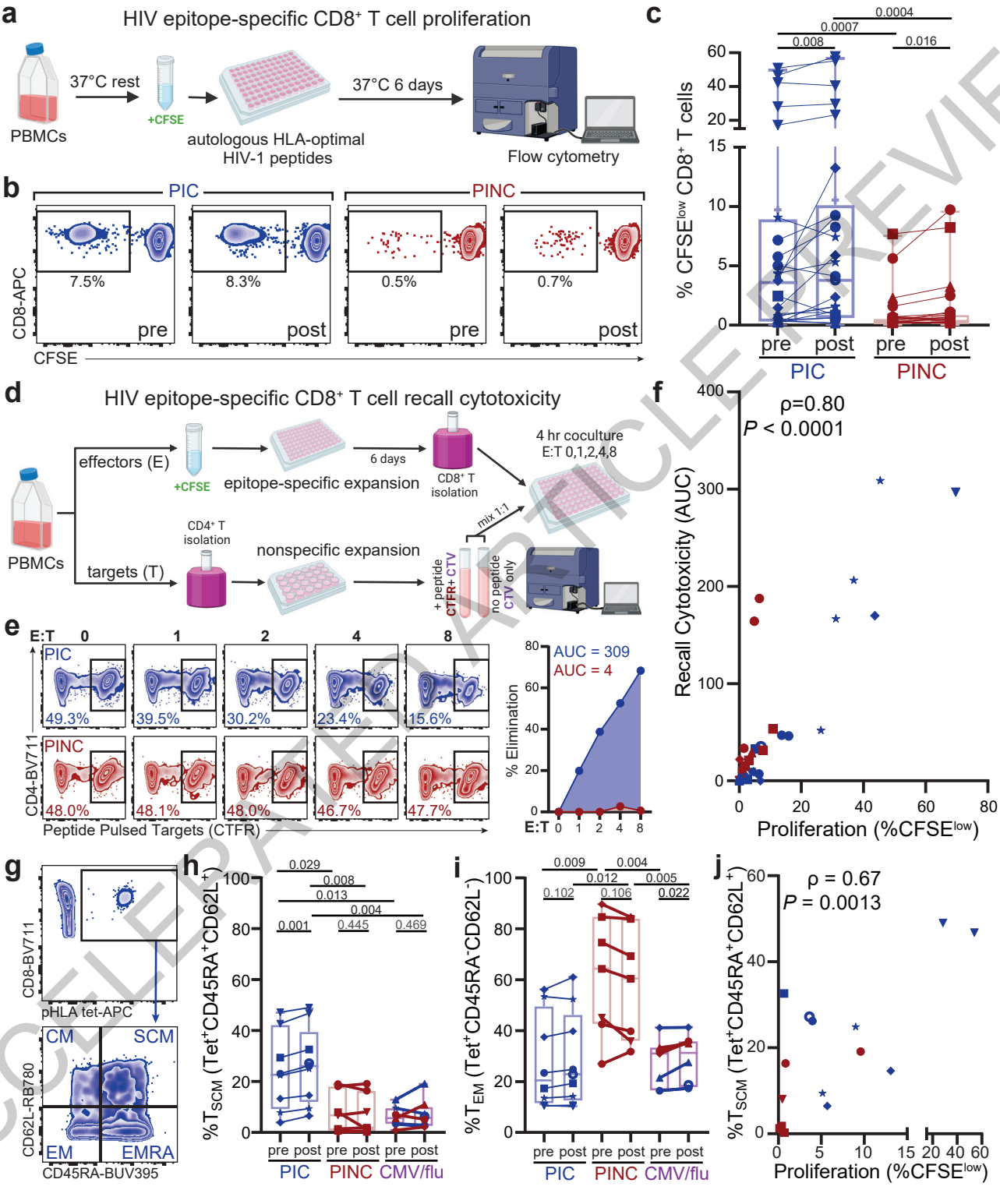

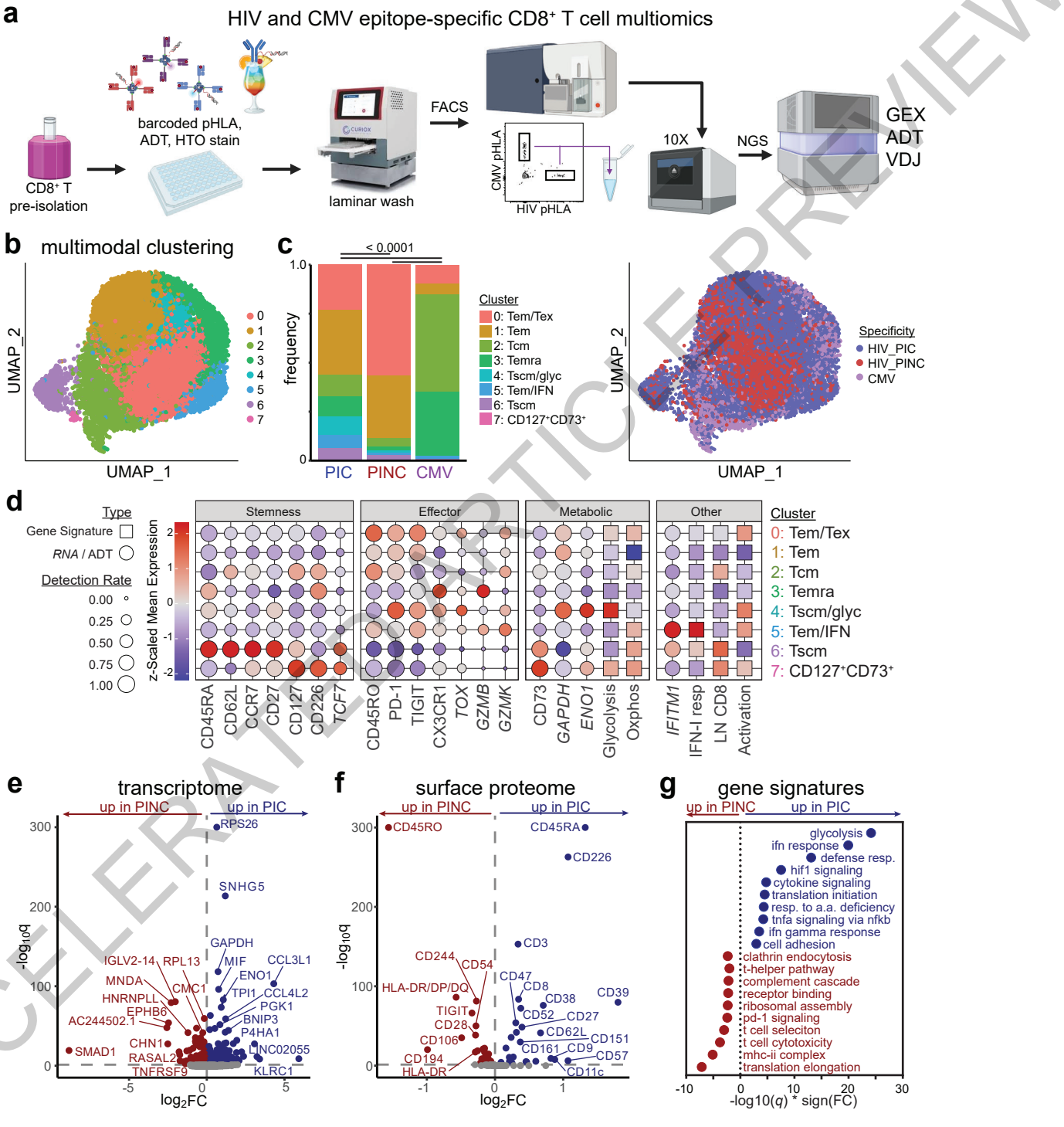

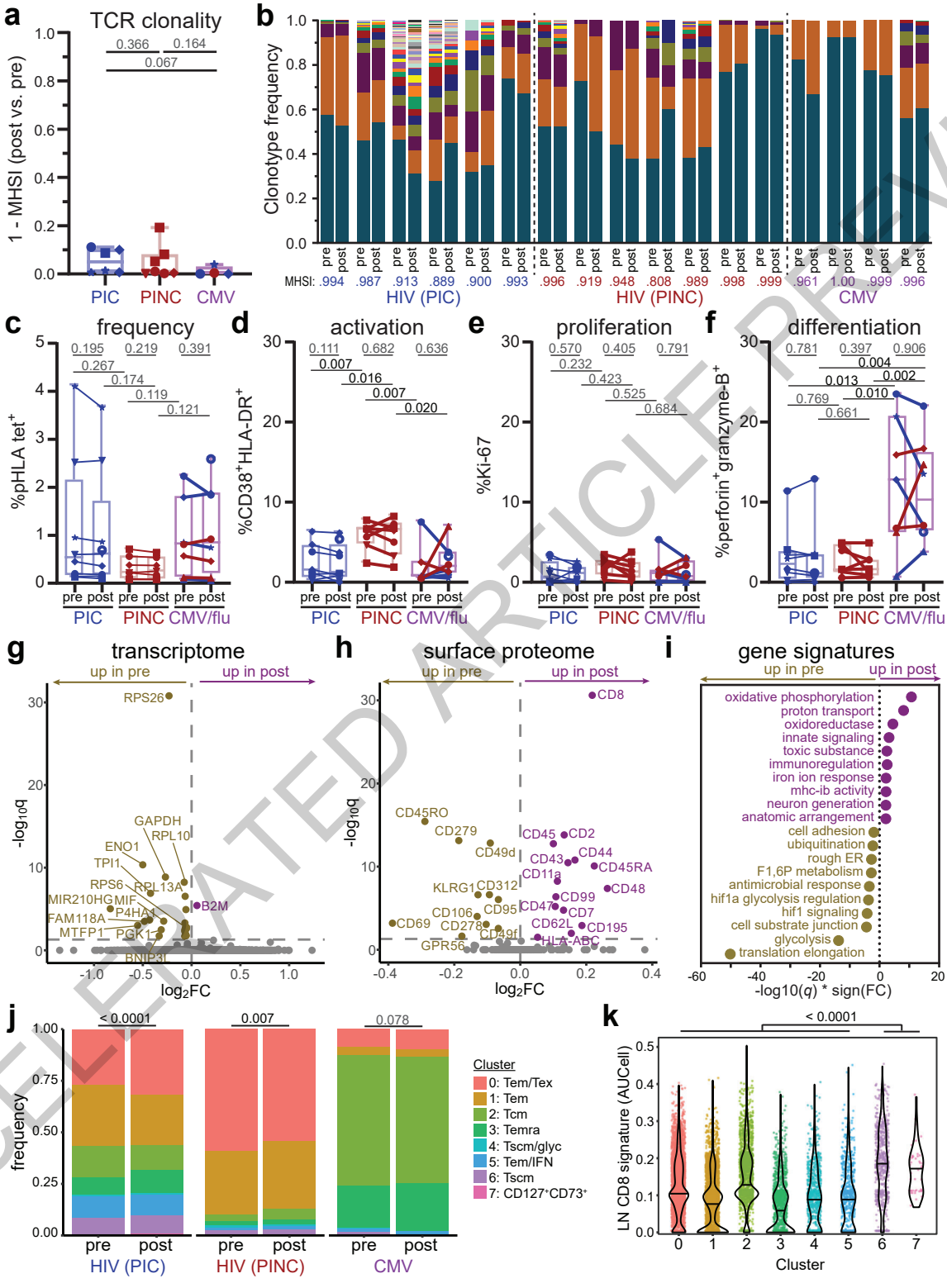

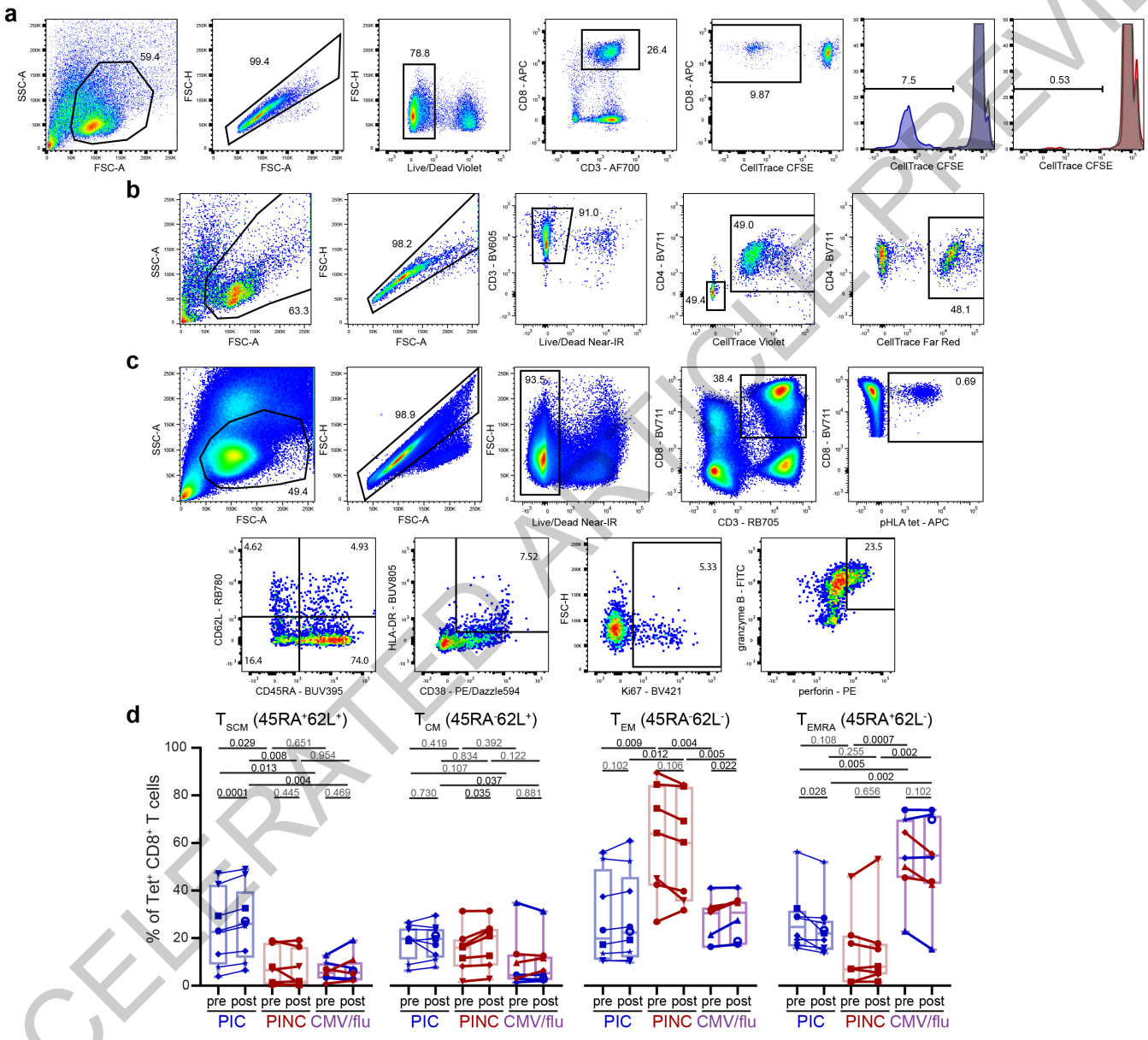

Extended Data Fig. 1

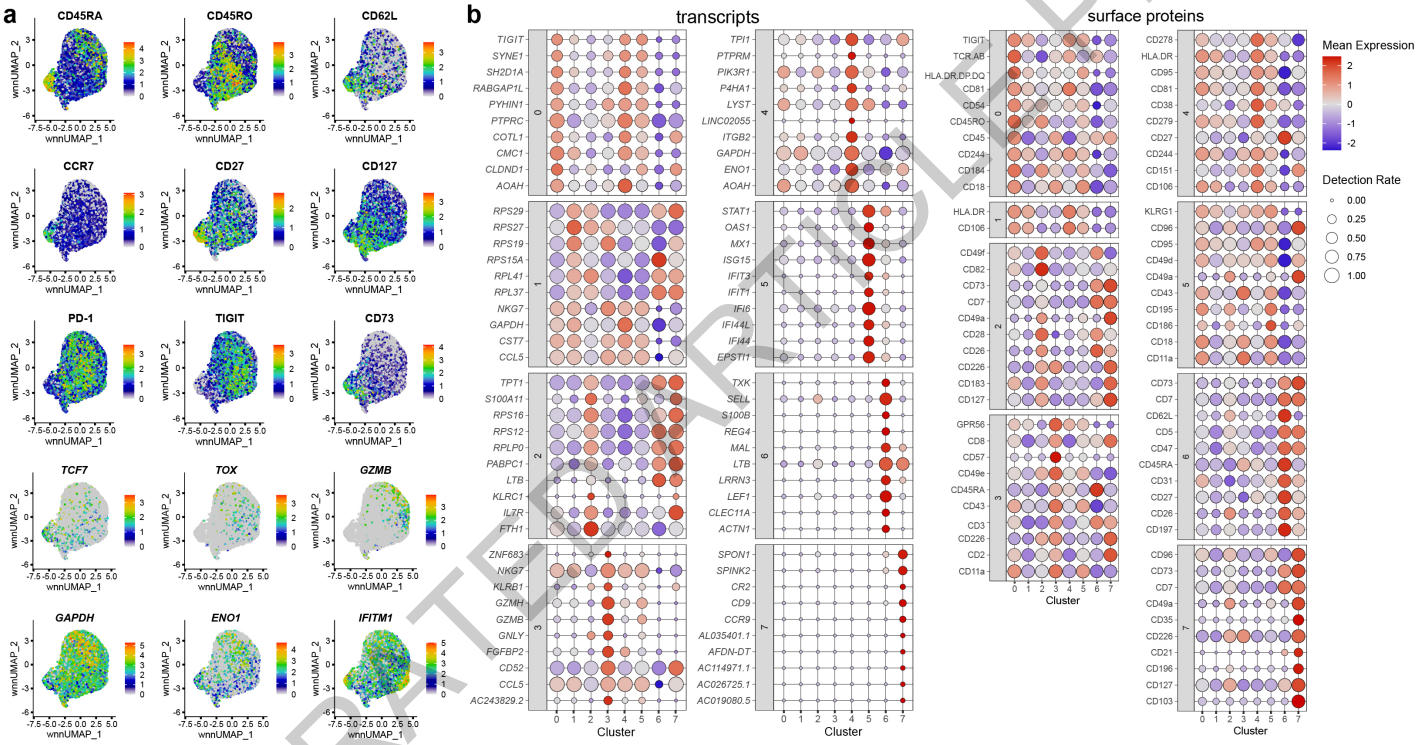

Extended Data Fig. 2

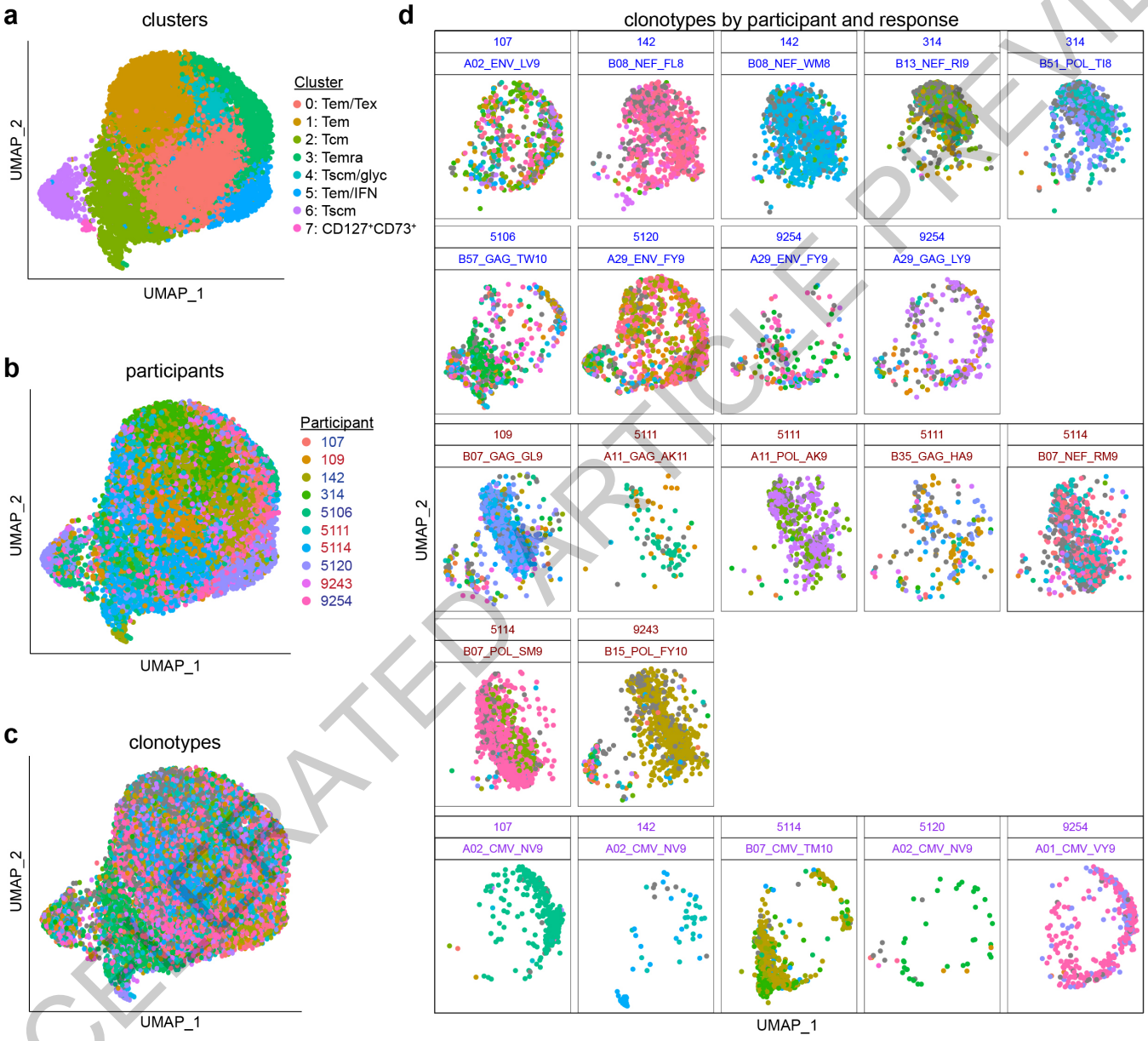

Extended Data Fig. 3

nature portfolio

Corresponding author(s): David R. Collins

Last updated by author(s): 10/10/2025

Reporting Summary

Nature Portfolio wishes to improve the reproducibility of the work that we publish. This form provides structure for consistency and transparency in reporting. For further information on Nature Portfolio policies, see our Editorial Policies and the Editorial Policy Checklist.

Statistics

For all statistical analyses, confirm that the following items are present in the figure legend, table legend, main text, or Methods section.

n/a	Confirmed
☐	☒ The exact sample size (*n*) for each experimental group/condition, given as a discrete number and unit of measurement
☐	☒ A statement on whether measurements were taken from distinct samples or whether the same sample was measured repeatedly
☐	☒ The statistical test(s) used AND whether they are one- or two-sided *Only common tests should be described solely by name; describe more complex techniques in the Methods section.*
☒	☐ A description of all covariates tested
☐	☒ A description of any assumptions or corrections, such as tests of normality and adjustment for multiple comparisons
☐	☒ A full description of the statistical parameters including central tendency (e.g. means) or other basic estimates (e.g. regression coefficient) AND variation (e.g. standard deviation) or associated estimates of uncertainty (e.g. confidence intervals)
☐	☒ For null hypothesis testing, the test statistic (e.g. *F*, *t*, *r*) with confidence intervals, effect sizes, degrees of freedom and *P* value noted *Give P values as exact values whenever suitable.*
☒	☐ For Bayesian analysis, information on the choice of priors and Markov chain Monte Carlo settings
☐	☒ For hierarchical and complex designs, identification of the appropriate level for tests and full reporting of outcomes
☐	☒ Estimates of effect sizes (e.g. Cohen's *d*, Pearson's *r*), indicating how they were calculated

Our web collection on statistics for biologists contains articles on many of the points above.

Software and code

Policy information about availability of computer code

Data collection	IFNG elispot data collection was performed using CTL ImmunoSpot Analyzer Pro version 7.0.38.16. Flow cytometric data collection and FACS were performed using BD FACSDiva version 9.2.
Data analysis	Flow cytometric data analyses were performed using FlowJo version 10.10.0. Statistical analyses were performed using GraphPad Prism version 10.4 and R version 4.3.1. Single-cell multiomics data analyses were performed using R version 4.3.1, cellranger version 9.0.0, bcl2fastq version 2.20, seurat version 5.3.0, tmod version 0.46.2, and GSNA version 0.1.4.9. Data visualizations were prepared using ggplot2 version 3.5.2 and Adobe Illustrator version 29.8.2.

For manuscripts utilizing custom algorithms or software that are central to the research but not yet described in published literature, software must be made available to editors and reviewers. We strongly encourage code deposition in a community repository (e.g. GitHub). See the Nature Portfolio guidelines for submitting code & software for further information.

Data

Policy information about availability of data

All manuscripts must include a data availability statement. This statement should provide the following information, where applicable:

- Accession codes, unique identifiers, or web links for publicly available datasets
- A description of any restrictions on data availability
- For clinical datasets or third party data, please ensure that the statement adheres to our policy

Full single-cell multiomics data are available via the NCBI Gene Expression Omnibus (GEO) via accession number GSE294440. The GRCh38 reference genome is available at NCBI GenBank via accession number GCA_000001405.15. MSigDB gene set references can be obtained from https://data.broadinstitute.org/gsea-msigdb/msigdb/release/7.5.1/. The remaining data are included within the manuscript and supplemental materials.

Research involving human participants, their data, or biological material

Policy information about studies with human participants or human data. See also policy information about sex, gender (identity/presentation), and sexual orientation and race, ethnicity and racism.

Reporting on sex and gender	Biological sex of each participant is reported in Table 1 as previously published for each parent trial.
Reporting on race, ethnicity, or other socially relevant groupings	Race (American Indian, Black, or White) and ethnicity (Hispanic or not Hispanic) of each participant are reported in Table 1 as previously published for each parent trial.
Population characteristics	Age, class-I HLA genotypes, and clinical histories related to HIV are reported for each participant in Table 1 as previously published for each parent trial.
Recruitment	This study includes only secondary use of previously collected samples.
Ethics oversight	Secondary use protocols were approved by the Mass General Brigham Human Research Committee

Note that full information on the approval of the study protocol must also be provided in the manuscript.

Field-specific reporting

Please select the one below that is the best fit for your research. If you are not sure, read the appropriate sections before making your selection.

☒ Life sciences ☐ Behavioural & social sciences ☐ Ecological, evolutionary & environmental sciences

For a reference copy of the document with all sections, see nature.com/documents/nr-reporting-summary-flat.pdf

Life sciences study design

All studies must disclose on these points even when the disclosure is negative.

Sample size	Sample sizes were constrained by specimen and reagent availability.
Data exclusions	Only participants who received intervention were included in the analyses. Participants/responses for which only one longitudinal sample was measured were excluded from longitudinal statistical comparisons. Doublets were excluded from multimodal single-cell analyses based on hashing and tetramer oligonucleotides. Cells with TCRs that occurred only once and cells for which TCR sequences were not detected were excluded from TCR clonotypic analyses.
Replication	Proliferation assays were confirmed in triplicate and averaged. Metrics were also repeated across longitudinal samples for each participant. The precise number of biological replicates is specified for each experiment in the figure legends and each data point is displayed in the figures. Representative data are only shown adjacent to the corresponding full data set for illustrative purposes. Further replication beyond those listed here were prohibited by limited specimen availability.
Randomization	This manuscript reports secondary analyses of specimens from previous trials. Experimental groups (PIC, PINC) were determined based on the presence or absence of prolonged virologic control without resumption of ART, as previously reported by each parent trial. Longitidinal samples (pre, post) were pre-determined based on which samples were collected prior to or following intervention in the parent trials. Viremia as a potential covariate was controlled by inclusion only of samples without detectable HIV viremia. Demographics are summarized in Table 1. Due to limited participant numbers, covariate modeling or controlling for additional potential covariates was not feasible.
Blinding	As this manuscript reports secondary analyses of specimens from previous trials, formal blinding was not part of the study design.

Reporting for specific materials, systems and methods

We require information from authors about some types of materials, experimental systems and methods used in many studies. Here, indicate whether each material, system or method listed is relevant to your study. If you are not sure if a list item applies to your research, read the appropriate section before selecting a response.

Materials & experimental systems

n/a	Involved in the study
☐	☒ Antibodies
☒	☐ Eukaryotic cell lines
☒	☐ Palaeontology and archaeology
☒	☐ Animals and other organisms
☒	☐ Clinical data
☒	☐ Dual use research of concern
☒	☐ Plants

Methods

n/a	Involved in the study
☒	☐ ChIP-seq
☐	☒ Flow cytometry
☒	☐ MRI-based neuroimaging

Antibodies

Antibodies used

anti-IFN-g, clone DK1, Mabtech, cat# 3420-2A, lot# 161; anti-CD3, clone OKT3, Biolegend, cat# 317326, lot# B407799; anti-CD28, clone CD28.2, Biolegend, cat# 302934, lot# B374639; anti-IFN-g, clone B6-1, Mabtech, cat# 3420-2A, lot#161; AlexaFluor700-anti-CD3, clone SK7, Biolegend, cat# 344822, lot# B420037; APC-anti-CD8, clone RPA-T8, Biolegend, cat# 301014, lot# B386144; BV605-anti-CD3, clone UCHT1, Biolegend, cat# 300460, lot# B430690; BUV395-anti-CD8, clone RPA-T8, BD Biosciences, cat# 563795, lot# 4292914; BV711-anti-CD4, clone RPA-T4, Biolegend, cat# 300558, lot# B420968; RB705-anti-CD3, clone UCHT1, BD Biosciences, cat# 570237, lot# 3229245; BV711-anti-CD8, clone RPA-T8, Biolegend, cat# 301044, lot# B425053; BUV395-anti-CD45RA, clone HI100, BD Biosciences, cat# 740298, lot# 5091519; RB780-anti-CD62L, clone DREG-56, BD Biosciences, cat# 569211, lot# 4200635; PE-Dazzle594-anti-CD38, clone HB-7, Biolegend, cat# 356630, lot# B406413; BUV805-anti-HLA-DR, clone G46-6, BD Biosciences, cat# 568335, lot# 4178322; PE-anti-perforin, clone B-D48, Biolegend, cat# 353304, lot# B397495; FITC-anti-granzyme B, clone GB11, Biolegend, cat# 515403, lot# B397296; BV421-anti-Ki-67, clone Ki-67, Biolegend, cat# 350506, lot# B356738; BV711-anti-CD8, clone RPA-T8, Biolegend, cat# 301044, lot# B425053; Total-Seq C Human Universal Cocktail v2.0, Biolegend, cat# 399910, lot# B408342; Total-Seq C anti-human hashtags 1-18, clone LNH-94/2M2, Biolegend, cat# 394661-394693, lot# B344497

Validation

Species reactivity and suitability for each application were validated by the commercial suppliers (Biolegend, BD Biosciences, Mabtech) for each antibody, with quality control certification provided for each lot.

Plants

Seed stocks

Report on the source of all seed stocks or other plant material used. If applicable, state the seed stock centre and catalogue number. If plant specimens were collected from the field, describe the collection location, date and sampling procedures.

Novel plant genotypes

Describe the methods by which all novel plant genotypes were produced. This includes those generated by transgenic approaches, gene editing, chemical/radiation-based mutagenesis and hybridization. For transgenic lines, describe the transformation method, the number of independent lines analyzed and the generation upon which experiments were performed. For gene-edited lines, describe the editor used, the endogenous sequence targeted for editing, the targeting guide RNA sequence (if applicable) and how the editor was applied.

Authentication

Describe any authentication procedures for each seed stock used or novel genotype generated. Describe any experiments used to assess the effect of a mutation and, where applicable, how potential secondary effects (e.g. second site T-DNA insertions, mosiacism, off-target gene editing) were examined.

Flow Cytometry

Plots

Confirm that:

☒ The axis labels state the marker and fluorochrome used (e.g. CD4-FITC).

☒ The axis scales are clearly visible. Include numbers along axes only for bottom left plot of group (a 'group' is an analysis of identical markers).

☒ All plots are contour plots with outliers or pseudocolor plots.

☒ A numerical value for number of cells or percentage (with statistics) is provided.

Methodology

Sample preparation

Cryopreserved PBMCs were thawed at 37 C and rested overnight in RPMI + 10% FBS prior to each assay.

Instrument

Data were collected using BD FACSSymphony A5, LSR-II, and FACSAria instruments.

Software

Collection was performed using BD FACSDiva. Analysis was performed using FlowJo.

Cell population abundance	Abundances of each cell population/subpopulation are reported for all flow cytometry and multiomics data as frequencies in the figures, extended figures, and supplementary data.
Gating strategy	Intact live CD8+ cells were gated on forward and side scatter, viability dye, and CD8. Elimination assay data were pre-gated on intact, live, CTV+ target cells. Gates are represented in manuscript figures.

☒ Tick this box to confirm that a figure exemplifying the gating strategy is provided in the Supplementary Information.